Ceramics International 46 (2020) 833–843

Contents lists available at ScienceDirect

Ceramics International

journal homepage: www.elsevier.com/locate/ceramint

A comparative study of physico-mechanical, bioactivity and hemolysis properties of pseudo-wollastonite and wollastonite glass-ceramic synthesized from solid wastes

SK S. Hossain[a], Sushma Yadav[a], Shreyasi Majumdar[b], S. Krishnamurthy[b], Ram Pyare[a], P.K. Roy[a,*]

[a] Department of Ceramic Engineering, IIT(BHU), Varanasi, 221005, UP, India
[b] Department of Pharmaceutical Engg. and Technology, IIT(BHU), Varanasi, 221005, UP, India

ARTICLE INFO

Keywords:
Wollastonite
Wastes
Eggshells
Rice husk ash
Hydroxyapatite
Hemolysis

ABSTRACT

This study aims to synthesize pseudo-wollastonite and wollastonite base glass-ceramic from solid wastes, and a comparative study of their physico-mechanical, bioactivity, and hemolysis properties is conducted. The stoichiometric amount of chicken eggshells derived CaO (~99%), and rice husk ash (RHA) derived nano SiO_2 (~99%) is used as ingredients for the formulation of wollastonite. The pseudo-wollastonite (α-W) is synthesized by sintering the ingredients at 1200 °C for 4 h, and wollastonite glass is made through the quenching method after melting of the ingredients at 1400 °C. The wollastonite glass-ceramic (GC) is prepared by control heat-treatment of wollastonite glass at 1200 °C for 1 h. Numerous characterizations like X-ray diffraction (XRD), scanning electron microscopy (SEM), apparent porosity and bending strength of α-W and GC are comparatively investigated. The GC is composed of the collaborative pseudo-wollastonite nucleation (~35%) and amorphous phases. α-W and GC show the apparent porosity about 4.23 % and 2.77 %, bending strength about 108 MPa and 139 MPa, and an average grain size about 2.30 μm and 0.60 μm, respectively. The obtained results exhibit that the waste-derived both α-W and GC have excellent bioactivity and good hemolysis index (< 2%). Moreover, GC shows slightly more hydroxyapatite (HA) layer formation ability than α-W in the simulated body fluid (SBF) solution. This comparative study of α-W and GC is recommended that the GC is offering more promising characteristics for biomedical applications.

1. Introduction

Wollastonite is a calcium-inosilicate mineral, which chemical formula is $CaSiO_3$. It belongs to the pyroxenoid group of white inorganic materials and consists of ~51.75 wt% of SiO_2 and ~48.25 wt% of CaO [1]. It has two polymorphic forms with the different crystal structure, the most common low temperature synthesized para-wollastonite (β-$CaSiO_3$) consists of a triclinic structure at around 1125 °C. Another is a high-temperature synthesized phase above at 1125 °C, i.e., pseudo-wollastonite (α-$CaSiO_3$) (α-W), consists of a monoclinic crystal system [2]. Some unique properties, i.e., high whiteness, low moisture absorption, low thermal expansion, low shrinkage, low dielectric constant and loss, fluxing properties, and thermal stability of wollastonite make useful in different industries include ceramics, chemicals, metallurgical, construction and polymers [3].

Last two decades, wollastonite bio-ceramic is also attracted in the field of orthopedics as an artificial bone implant or tissue repair for their unique properties like bio degradability, excellent bioactivity, nontoxicity, and biocompatibility [4–6]. It has exhibited strong ability for the formation of apatite layers on their surfaces in simulated body fluid (SBF), artificial saliva, cell culture medium, and *in vivo* environments. These apatite layers play an important role for tight bonding between the host bone tissues and implants [7–9]. Therefore, wollastonite is used as a bioactivity improving agent in different bio-inert materials such as, ceramics, polymers, and metals, which have been used in various medical applications, particularly for orthopedics. Aly et al. [10] have been prepared a nano-fiber bio-ceramic composite of wollastonite/titanium oxide for bone substitute implant. They have proposed that this composite shows well *in vitro* bioactivity with high mechanical strength, which can be substituted for high load bearing site bones. Li et al. [11] have been fabricated a wollastonite coating on titanium alloy (Ti6Al4V) by laser cladding for improving the bioactivity. Titanium alloys generally use as implant materials due to their superior mechanical and excellent corrosion resistance properties.

* Corresponding author.
E-mail address: pkroy.cer@iitbhu.ac.in (P.K. Roy).

https://doi.org/10.1016/j.ceramint.2019.09.039
Received 29 May 2019; Received in revised form 2 September 2019; Accepted 3 September 2019
Available online 05 September 2019

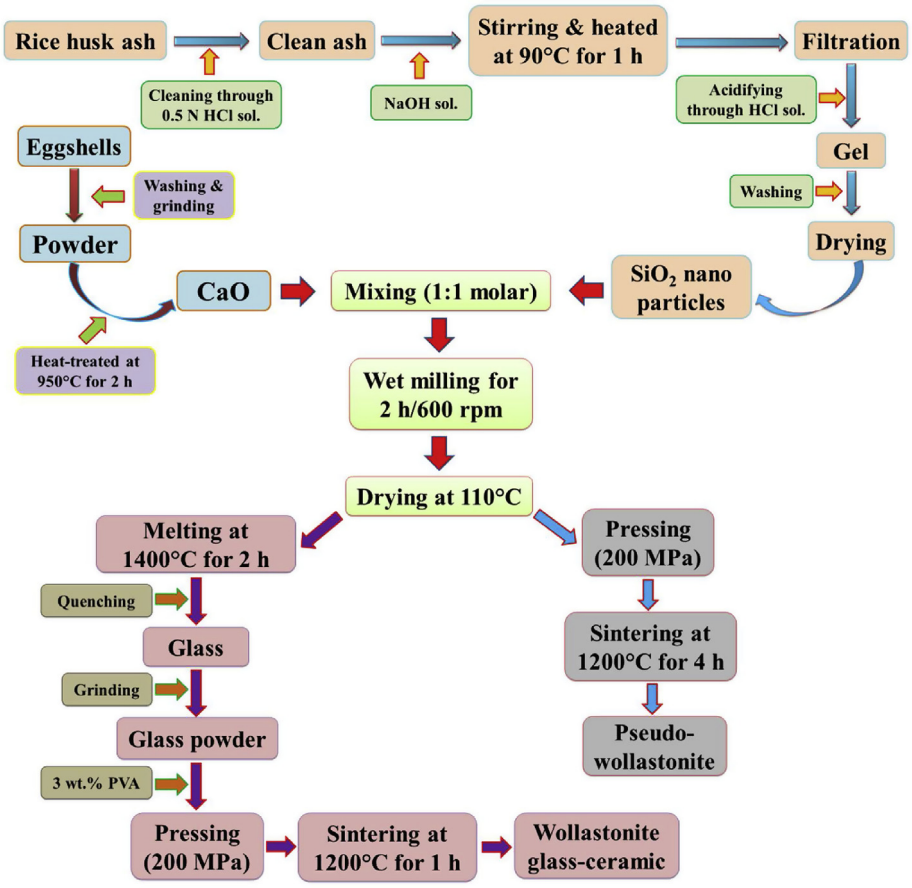

Fig. 1. Preparation scheme of CaO, nano SiO_2, α-wollastonite and wollastonite glass-ceramic.

Saravanan and Selvamurugan [12] have been investigated the bone healing ability of mesoporous wollastonite. They have suggested that the porous wollastonite particles have good bioactive properties and used as a filling material for the elevation of bone regeneration *in vivo*. Lin et al. [13] have been fabricated calcium silicate micro spheres, which show excellent apatite formation ability with promising drug release property. They have proposed that the microspheres calcium silicate is favorable for drug delivery as an injectable filling material for bone formation. Nevertheless, a different form of wollastonite is exhibited different properties like apatite formation mechanism, mechanical strength, and physical characteristics. Therefore, an investigation is required to analyze which form (β-wollastonite, α-wollastonite, or wollastonite glass-ceramics) is the most efficient for a particular application. Several researchers have studied the bioactivity characteristics of β-wollastonite [14], α-wollastonite [15], and wollastonite glass-ceramics [16]. Rodriguez et al. [17] and Morsy et al. [18] have studied the bioactivity of β-wollastonite and α-wollastonite and compared their bioactivity. To the best of our knowledge, no such investigation has been found to compare the study of bioactivity of α-wollastonite and wollastonite glass-ceramics (GC). Glass-ceramics refer to a composite material constituted of crystals in its glassy matrix. The controlled heat-treatment develops the crystallinity through nucleation and growth process in a base glass, which is depicted the unique properties than amorphous or crystalline states of respective compositions [19].

On the other hand, the world demands for high purity, low-cost wollastonite for orthopedics application, and its requirement are gradually expanding. Naturally occurring wollastonite contains a small amount of manganese, magnesium, and iron [20]. Thus, many researchers have described several advanced preparation routes, including sol-gel, co-precipitation, thermal decomposition, and hydrothermal method for the synthesis of high purity synthetic wollastonite [21–23]. However, the use of expensive and toxic raw materials and complicated processing methodology are constrained to the commercialization of these methods. Nowadays, researchers are trying to find alternative processes, which consist of less expensive, non-toxic, and abundantly available raw materials. Azam et al. [24] and Shamsudin et al. [14] have synthesized α-wollastonite and β-wollastonite, respectively, from rice husk ash and limestone. Rashid et al. [25] have produced wollastonite from limestone and silica sand. Fiocco et al. [26] have reported porous wollastonite for bone regeneration from polymer. Present work is carried out to fabricate high purity synthetic α-wollastonite, and wollastonite glass-ceramic from 100% abandoned solid waste, i.e., rice husk ash (RHA) and eggshells through conventional solid-state route.

Rice industry produces around ~20 wt% rice husk (RH) as a by-product. It is mainly used in the boilers as a fuel to generate energy through the gasification or by direct combustion [27]. After incineration of RH, new waste, i.e., rice husk ash (RHA) is generated around 18–25 wt%. This waste has no particular uses rather than land-filling [28]. Moreover, RHA contains around 90 wt% of amorphous silica, which has a huge potential to replace the traditional sources of silica [29]. Eggshells are found as waste from food making industries. It is disposed of in huge amounts every day and spread bad smells that create pollution or public health issues. Chicken eggs contain around ~11 wt% of shells of the total weight of eggs. It contains about ~94 wt % calcium carbonate, 1 wt% tri-calcium phosphate, 1 wt% magnesium carbonate, and remaining part mainly organic matter [30]. The availability and chemical composition of RHA and eggshells indicate that they can be used as an alternative source of silica and calcium, respectively instead of natural ingredients for synthetic wollastonite formulations.

The present work is carried out to investigate the possibility of using waste eggshells, and rice husk ash derived SiO_2 as ingredients for preparing of α-wollastonite and wollastonite glass-ceramic, which may find suitable application for biomedical fields. The importance is given to the synthesis of α-wollastonite and wollastonite glass-ceramic, and their physico-mechanical, bioactivity and blood compatibility properties. The investigation deals with eco-friendly, sustainable bio-ceramics for biomedical applications.

2. Experimental procedures

2.1. Raw materials synthesis

The preparation scheme of CaO from eggshells, nano SiO_2 from RHA, α-W, and GC are depicted in Fig. 1. At first, eggshells were collected from a local restaurant, and then it was washed in tap water. The shells were dried in sunlight and ground in a ball mill for about 1 h at 300 rpm with a weight ratio of powder to balls of about 1:10. Later, the ground powder was calcined at 950 °C for 2 h in a muffle furnace and yielded a pure calcium oxide (~99%). Silica was extracted from RHA through alkali extraction method, which is deeply described in our previous publication [31]. First, RHA was collected from Samrat rice mill, Burdwan, India where, rice husk was used as a fuel in the boiler. The RHA was cleaned with 0.5 N HCl solutions to remove minerals and dirts. Then, 20 gm of clean dry RHA was mixed with 27 gm of NaOH (assay 99%) pallet in 200 ml water and heated at 90 °C for 1 h with continuous magnetic stirring. It was then left for 24 h at room temperature for completion of the reaction (reaction 1), and the silicate solution was filtered from the mixture through the Millipore filter papers. The filtrate was acidified by addition of HCl solution until the sol was completely transformed into a gel (reaction 2). The formed gel was left for aging for 1 day, and then deionized water was used for washing to eliminate the excess other ions. The obtained gel was then dried at 110 °C for 10 h and ground into fine SiO_2 powder. The following reactions are taking place during the silica extraction from RHA:

$$SiO_2(RHA) + 2NaOH \rightarrow Na_2SiO_3(aq.\ ) + H_2O \quad (1)$$

$$Na_2SiO_3 + HCl \rightarrow SiO_2(gel) + NaCl(aq.\ ) + H_2O \quad (2)$$

2.2. Wollastonite synthesis

The pseudo-wollastonite was synthesized by the conventional solid-state route through the mixing of stoichiometric (1:1 M) ratio of calcined eggshells (~99% CaO), and RHA extracted SiO_2 (~99% SiO_2) as ingredients. Mixed mass was wet milled in a planetory ball mill (Model No: MBM-07, Insmart Systems, Hyderabad, India) using high purity zirconia balls of 5 mm diameter for 2 h with 600 rpm in water as a medium. For pelletization, the wet mixture was dried at 110 °C for 5 h, and the dry powder was pressed at a pressure of 200 MPa under the uniaxially hydraulic pressed. The green plates were sintered in a controlled muffle furnace (Bysakh & Co, Kolkata, India) at 1200 °C for 4 h with a heating and cooling rate of 3 °C/min.

2.3. Wollastonite glass ceramic synthesis

The calcined eggshells and RHA derived silica (1:1 M ratio of CaO and SiO_2) was wet-mixed in a ball milled for 2 h with 600 rpm in water as a medium. After mixing, this material was transferred into the platinum crucible of capacity 30 ml and melted at 1400 °C for 2 h in a globar furnace with air atmosphere. The molten mass was then quickly transferred into distilled water containing aluminum bowl to protect the possibility of crystallization (quenching method), and yielded with transparent glass. The wollastonite glass was grounded and passed through 60 μm sieve. The glass powder was pressed by a uniaxially hydraulic pressed at a pressure of 200 MPa after mixing 3 wt% of PVA as a binder. The pressed plates were heat-treated in a controlled muffle furnace at 1200 °C for 1 h with a heating and cooling rate of 10°/min.

2.4. Characterizations

The chemical compositions of RHA derived SiO_2, and calcined eggshells were evaluated by the X-ray fluorescence (XRF) spectrometer (Philips PW 2400, Netherlands). The present phases in the waste RHA derived silica, calcined eggshells, synthesized α-W, and GC were examined by X-ray diffraction (XRD) analysis carried out through the X'Pert Pro diffractometer equipped with Ni filter and Cu-kα (1.5406 Å) radiation, the step size of 0.02° in the range of 10°–80° with 3°/min scanning rate. The percent of crystallinity (CI) developed in the glass-ceramic was evaluated by the ratio of the crystalline area (CA) to the total area (TA) (TA = amorphous area + crystalline area) in the XRD diagram of the glass-ceramics [32], by using the following equation (3):

$$CI\% = {}^{CA \times 100}/_{TA} \quad (3)$$

The functional groups present in α-W and GC were analyzed at room temperature in the range of frequency 4000–400 cm^{-1} using a Fourier transform infrared spectrometer (FTIR) (BRUKER, TENSOR 27-3772) by the attenuated total reflection (ATR) method. The particle morphology of RHA derived SiO_2 and calcined eggshells, along with surface morphology of α-W and GC samples were carried out using a scanning electron microscope (FEI, Nova Nano SEM 450, Netherlands). Particles size of RHA derived SiO_2 was measured by the transmission electron microscopy (TEM) (FEI, TECNAI G2-20 TWIN, Netherlands). The apparent porosity (AP) and bulk density (BD) of the synthesized α-W and GC was measured according to ASTM C20. Three-point bending strength of α-W and GC specimens was done according to ASTM C133 (UTM, H10KL-I0129).

Simulated body fluid (SBF) solution was prepared according to Kokubo and Takadama [33] to study the *in vitro* bioactivity of α-W and GC. The ion concentrations in SBF solution were similar to human blood plasma. The SBF solution was synthesized by dissolving the required amount of reagent grade NaCl, $NaHCO_3$, Na_2SO_4, KCl, $MgCl_2{\cdot}6H_2O$, $K_2HPO_4{\cdot}3H_2O$, and $CaCl_2$ in double distilled water and the solution was buffered at pH~7.4 with TRIS (trishydroxy methyl amino methane) and 1 N HCl solution at 37 °C. For performing the *in vitro* bioactivity test, 0.25 gm of each sample was kept in a bacteriological polyurethane incubator with 25 ml (10 mg/ml) SBF solution at 37 °C for 1, 3, 5, 7, 10, 14, 21 and 28 days to study the different levels apatite formation. During soaking, the change of pH value of SBF solution was measured through a digital pH meter (Toshcon Industries Pvt. Ltd., Ajmer, India). After soaking, the specimens were filtered from SBF solution, rinsed with distilled water and then dried at 40 °C for 5 h in an electric air oven. The formation of an apatite layer on the α-W and GC surface was examined by the XRD, FTIR, SEM, and energy-dispersive X-ray (EDX) analysis.

The hemolysis assay analysis was performed according to ASTM F 756-00 [34]. α-W and GC specimens with 7 ml of phosphate-buffered saline (PBS) for each test were added in polypropylene tube and incubated for 72 h at 37 °C. Later, the PBS solution was removed, and 1 ml diluted blood (9.02 mg/mL) of acid citrate dextrose (ACD) rat venous was added to each specimen at 37 °C for 3 h. Positive (+ve) and negative (-ve) controls were organized by mixing the same amount of ACD blood with 7 mL of distilled water and PBS, respectively. For proper contact of material with blood, the tubes were carefully upturned twice within 30 min interval. After incubation, the fluids were transferred into the centrifuge tube and centrifuged at 2000 rpm for 15 min. The hemoglobin was unconfined by hemolysis, which was recorded by the optical densities (OD) of the aliquot at 540 nm using a Micro-plate Reader, Synergy HT Multi-Mode (BioTek, USA). All tests were performed three times for better accuracy. The following equation was used to measure the percentage of hemolysis:

Table 1
Chemical composition of calcined eggshells and alkali extraction silica from RHA.

Compound (wt.%)	Calcined eggshells	Silica
SiO_2	-	99.32
Na_2O	0.17	0.31
P_2O_5	0.23	0.11
K_2O	-	0.08
CaO	99.08	0.07
Fe_2O_3	0.08	0.05
TiO_2	-	0.02
MgO	0.29	0.04
SrO	0.15	-

$$\%\ hemolysis = \frac{OD_{sample} - OD_{negative\ control}}{OD_{positive\ control} - OD_{negative\ control}} \times 100 \quad (4)$$

3. Results and discussion

3.1. Characterization of raw materials

The discussion about RHA and eggshells were reported in our previous study [35]. Table 1 illustrates the chemical compounds present in the calcined eggshells, and RHA extracted silica. It contains above 99 wt % of CaO and SiO_2, respectively. Fig. 2(a) shows the XRD image of calcined eggshell, and it is composed of mainly calcium oxide [CaO] and portlandite [$Ca(OH)_2$]. The humidity of the atmosphere may be causing the formation of portlandite in calcined seashells. A similar result was also observed by Leite et al. [36]. The SEM micrograph of calcined eggshell powder is shown in Fig. 3. The powder is contained mostly of unevenly shaped particles with an average size of 0.87 μm as calculated by "linear intercept method" from SEM image through "Image-J1.48V″ software.

Fig. 2(b) describes the XRD analysis of RHA extracted silica. It is shown only a broad peak, centered at around 22°, which represents the existing of SiO_2 (JCPDS 47-0715) [37]. Consequently, absences of any sharp diffraction peaks in the pattern indicate that it's amorphous in nature [38]. Fig. 4(a) and (b) depictes the SEM and TEM micrograph of RHA extracted silica. Both images exhibit that the silica particles are nearly spherical in shapes with bad agglomeration. This is due to the high ratio of surface to volume of silica particle, and it is ascribed to the strong attractive forces between the silica particles. Therefore, particles are agglomerated, and the average size of the particle is attributed

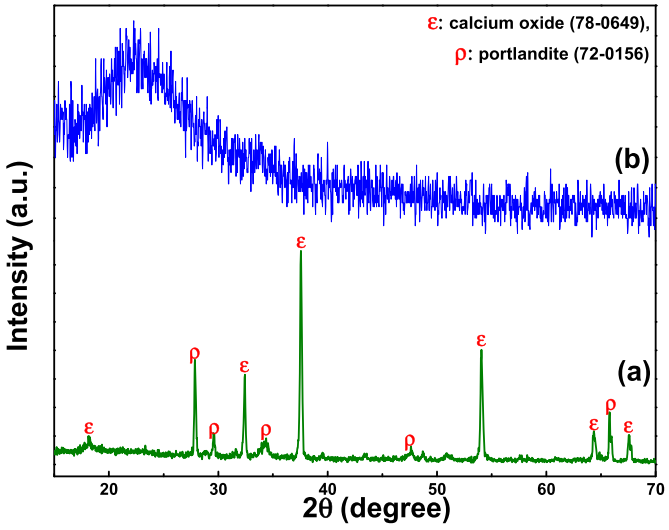

Fig. 2. XRD analysis of (a) calcined eggshells and (b) RHA derived nano SiO_2.

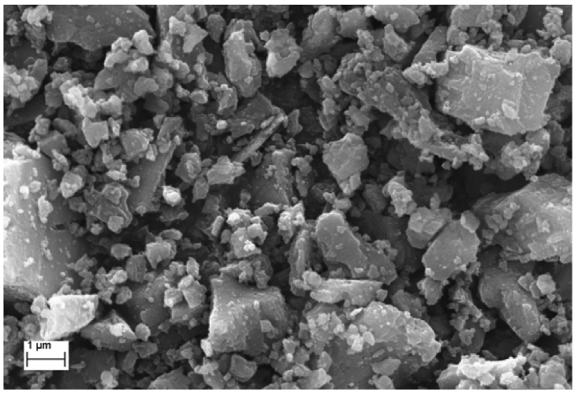

Fig. 3. SEM micrograph of calcined eggshells powder.

around ~25 nm.

3.2. Characterization of wollastonite and wollastonite glass-ceramic

Fig. 5(a) shows the room temperature XRD of sintered wollastonite at 1200 °C. From this figure, it is confirmed the formation of a pure phase of wollastonite. The highly active amorphous nano-SiO_2 and eggshells derived active CaO is more potentially reacted with each other through diffusion reaction and forms a pure wollastonite phase. Any unreacted silica and calcium oxide are not detected in the system. Mainly the pseudo-wollastonite, i.e., α-wollastonite (anorthic, C-1) phase is attained at 1200 °C sintered wollastonite samples. However, an insignificant amount of untransformed para-wollastonite, i.e., β-wollastonite (monoclinic, P21/a) phase is also observed in the system. Above 1100 °C, wollastonite phase is undergone through a polymorphic transformed reaction, i.e., low-temperature phase (β-wollastonite) to high-temperature phase (α-wollastonite) [39]. The eutectic invariant point in CaO-SiO_2 binary system is around 1500 °C for 1:1 M ratio of CaO and SiO_2 [40]. However, in this work, glass was melted lower than the eutectic point. This is due to eggshell and RHA, which contains more active CaO and SiO_2 (amorphous) than conventional sources, respectively. Further, the fineness of ingredients is also greatly affecting the melting temperature of material [41]. Therefore, nano silica (~25 nm) and micro calcium oxide (~0.87 μm), may be accelerated the reaction, and it's melted at low temperature than the eutectic invariant point.

Fig. 6(a) shows the XRD analysis of wollastonite glass, and the absence of any crystalline peak demonstrates that the melted wollastonite at 1400 °C is transferred into a purely amorphous form. However, some crystallinity is developing in the wollastonite glass after heat-treatment at 1200 °C, as shown in Fig. 6(b) and the value of CI% is around ~35%. The formed crystals contain purely pseudo- wollastonite phase identified through the JCPDS No 74-0784. Therefore, at 1200 °C heat-treated glass is composed of collaborative pseudo-wollastonite and amorphous phases, which may be called 'α-wollastonite glass-ceramic.'

The presence of chemical bonds in the α-W and GC are analyzed through FTIR analysis, as shown in Fig. 7(a) and Fig. 8(a), respectively. The peak at around 990 cm^{-1} is recognized to the asymmetric stretching vibration of Si-O-Si bridge bonds in [SiO_4]-tetrahedra. Consequently, symmetrical stretching vibrations of Si-O bands are attributed through the strong absorption region at about 650–960 cm^{-1} [21]. The bending vibrations of Si-O group are assigned by the peak in between 450-600 cm^{-1} spectrum. The peak confirms the [CaO_6]-octahedra in the structure at 423-450 $cm^{-1}$and 940 cm^{-1} [13]. The characteristic bonds of Ca-O-Si are assigned through broadband at about 860 cm^{-1} [22].

The surface morphology of α-W and GC are shown in Fig. 9(a) and (b), respectively. It can be observed that both exhibit a dense structure, but the size and shape of the grains are different. The average grain size

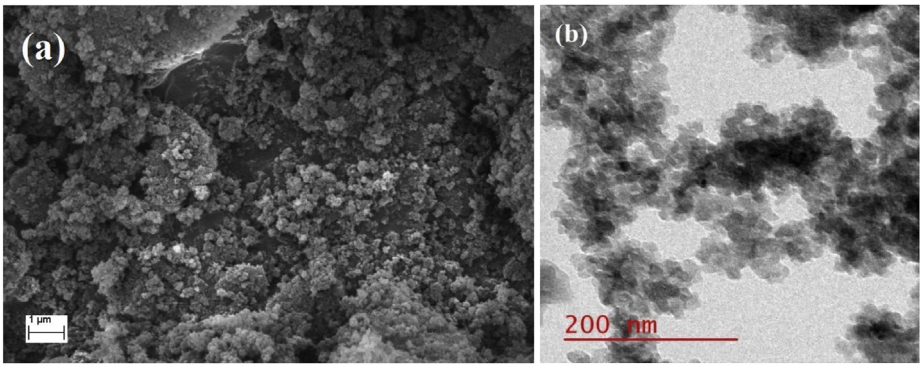

Fig. 4. (a) SEM and (b) TEM images of waste RHA derived silica.

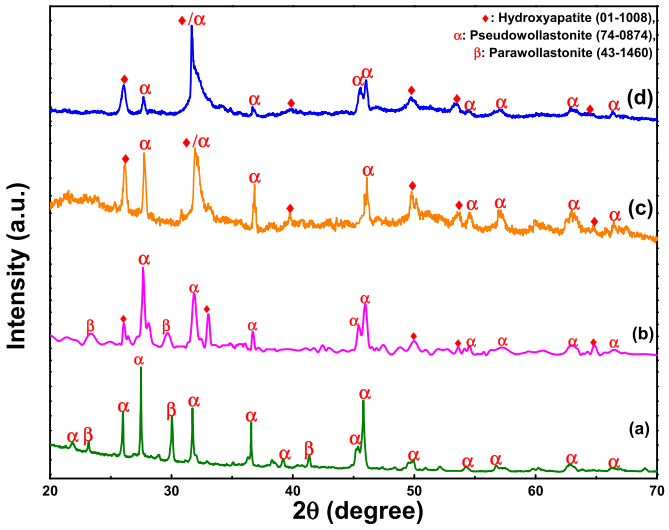

Fig. 5. XRD pattern of α-wollastonite (a) before soaking in SBF and (b) after soaking in SBF for 7 days, (c) 14 days and (d) 28 days.

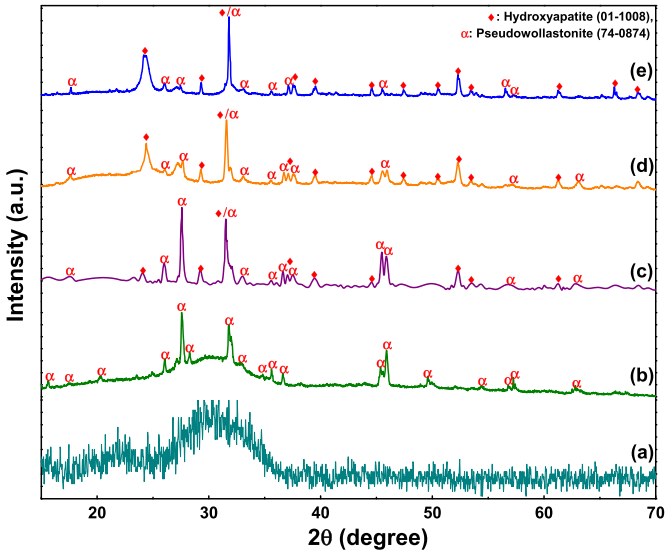

Fig. 6. XRD pattern of (a) wollastonite glass, (b) glass-ceramic before soakingin SBF and (c) after soaking in SBF for 7 days, (d) 14 days and (e) 28 days.

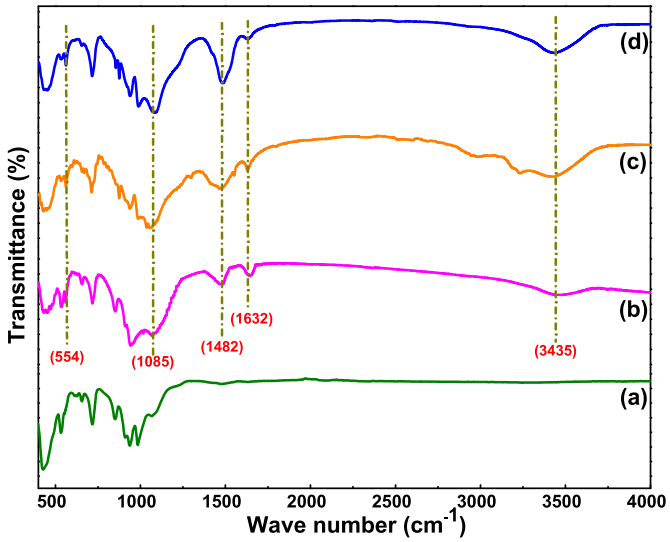

Fig. 7. FTIR spectrum of wollastonite (a) before soaking in SBF and (b) after soaking in SBF for 7 days, (c) 14 days and (d) 28 days.

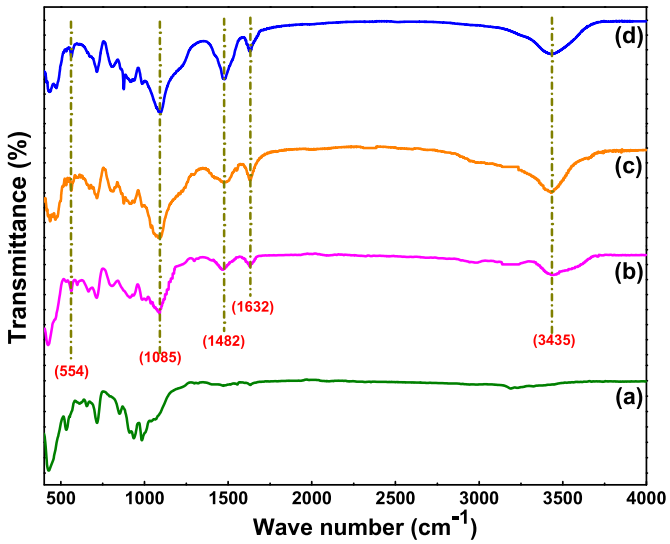

Fig. 8. FTIR spectrum of wollastonite glass-ceramic (a) before soakingin SBF and (b) after soaking in SBF for 7 days, (c) 14 days and (d) 28 days.

of α-wollastonite is around 2.30 μm, and the shape is uneven. Consequently, the glass-ceramic contains small size (~0.60 μm) grains than α-wollastonite with nearly spherical in shape and some glassy phases. It may be happened due to wollastonite glass, which starts crystallization at around 1051 °C [42] through the homogeneous nucleation mechanism, and its rate is very slow. However, the formed nucleus starts to grow at 1200 °C but, lack of time to grow the nucleus and transformation of glass to crystal is stopped. Therefore, the size of formed

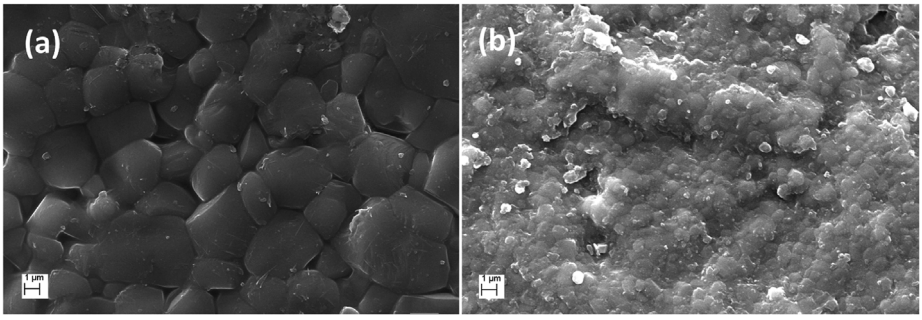

Fig. 9. SEM micrograph of (a) wollastonite and (b) glass-ceramic.

Table 2
Apparent porosity, bulk density and bending strength of sintered samples.

Samples	Apparent porosity (%)		Bulk density (gm/cc)		Bending strength (MPa)	
	Mean	s.d.	Mean	s.d.	Mean	s.d.
Wollastonite	4.23	0.58	2.562	0.093	108.35	8.70
Glass-ceramic	2.77	0.47	2.623	0.074	139.57	11.60

grains in glass-ceramic is lower than purely crystalline wollastonite. Some unconverted amorphous phases are present in the system, as shown in Fig. 6 (b).

The mean values for apparent porosity, bulk density, and bending strength of pseudo wollastonite and glass-ceramic are illustrated in Table 2. Both samples have exhibited low porosity than previously reported values in different studies, where wollastonite was synthesized from conventional ingredients and different low melting oxides, which were used to decrease the porosity as a sintering aid [43,44]. In this study, the uses of the solid-waste (eggshell and rice husk) derived reactive precursors are the main reason to lower the porosity of sintered wollastonite and glass-ceramic. However, slightly lower porosity is found in glass-ceramic specimens than wollastonite. It may be resulted due to the amorphous and crystalline particles, which are densifying through different mechanisms, i.e., viscous flow and diffusion, respectively [45]. The principle of viscous sintering is quietly simple and more effective for densification than diffusion mechanism, and it could be attributed to a more dense body. Consequently, the bending strength of GC is significantly higher than α-W. It can be ascribed due to GC specimen contains the small size of grains and low porosity. Small size grains have introduced the number of the grain boundary, which inhibits the crack propagation through the system. Additionally, lower porosity of GC is reduced the number of cracks and its propagation site. These results in the higher strength value of GC than α-W. However, the bending strength values of both GC and α-W are comparable, and both have above the minimum required value for human cortical bone application [46,47].

3.3. Characterization of samples after soaking

Fig. 5(b–d) and Fig. 6(c–e) show the room temperature XRD analysis of α-W and GC, respectively, after soaking in SBF solution. It can be observed that the intensity of α-W phases is reduced with soaking time for both the samples. It is attributed due to the formation of hydroxyapatite (HA) phase on the surface of α-W and GC. The formation of HA phase is confirmed through the characteristic peak of HA at around $2\theta = 32^{\circ}$ [16]. Consequently, the number of HA peaks increases with soaking period 7–28 days. It indicates that the amount of HA precipitation on the surface is increased. By comparing the number of HA peaks in Figs. 5(d) and Fig. 6(e), it is confirmed that the GC is more degradable than α-W in SBF solution. Therefore, the result shows that the GC has more HA formation capability than α-W.

The α-W and GC are characterized through FTIR analysis before and after soaking in SBF solution, and the results are presented in Fig. 7(b–d) and 8 (b-d), respectively. FTIR spectrum for before soaking in SBF are discussed earlier in "characterization of wollastonite and wollastonite glass-ceramic" section. After soaking in SBF, some newly peaks have appeared in the spectrum at 554, 1085, 1482, and 1632 cm^{-1}. The broad peak center at 1085 cm^{-1} and a minor peak at 554 cm^{-1} could be ascribed to the stretching and bending of phosphate groups (PO_4^{3-}) of the formed apatite layers, respectively. The carbonate groups (CO_3^{2-}) are assigned through the 1482 cm^{-1} band [48]. The minor peak at 1632 cm^{-1} and broadband center at 3435 cm^{-1} ensure the existence of O-H groups in the system [13]. This study further confirms that the formation of hydroxyl carbonate apatite (HCA) layers on the surface of the specimens after soaking in SBF solution. Consequently, the intensity of characteristic absorption bands in the FTIR spectrum is significantly increased with the soaking time (7–28 days) in SBF and increase the HCA layers concentration. The ability of HCA formation on the surface is essential for a bioactive material. It is playing an important role to develop the tight chemical bonds between the neighboring tissues, and bioactive materials derived implant [8,9]. Thus, the results of FTIR analysis have suggested that the solid wastes derived α-W and GC both have excellent bioactivity and excellent material for biomedical application.

Fig. 10 illustrates the surface morphology of α-W and GC samples after soaking in SBF solution for different periods. It has been seen that the surfaces of both specimens are significantly changed after soaking for 7 days in SBF. The surface of α-W and GC are fully covered with fine needle-like HA particles. In comparing the surface characteristic of α-W and GC (Fig. 10), significant change doesn't observe for 7 days soaking; both contain less than 30 nm diameter worm-like apatite particles. However, different changes are observed in the size and shape of the apatite particles that are deposited on α-W and GC samples with soaking periods. After 28 days of soaking, both samples show different surface morphology. The growth of apatite particles is uneven in GC. It indicates a rough surface of amorphous layers and needle-like crystalline apatite's. Consequently, α-W attributes a dense layer with nearly spherical in shape apatite particles.

The elemental mapping images of α-W and GC for 28 days soaking specimens are depicted in Fig. 11 (a) and (b), respectively. It is observed that the P and Ca element are uniformly distributed on the surface, and these elements are the main constituents for the formation of HA. The present analysis is another evidenced to the formation of HA layer on the surface of α-W and GC samples.

The variation of pH values in SBF solution with a soaking time of specimens is shown in Fig. 12. Before soaking, pH value of SBF solution is 7.4, which is nearly equal to the human blood plasma [33], and this value increases with soaking time. The pH values of α-W and GC after 5 days reach up to 8.35 and 8.52, respectively. This is attributed due to ion exchange in between of Ca^{2+} ions in material and H^{+} or OH^{-} ions in SBF solution through the succeeding reaction [49]:

$$CaSiO_3(s) + H^{+}(aq.\ ) \rightarrow HSiO_3^{-}(aq.\ ) + Ca^{2+}(aq.\ ) \quad (5)$$

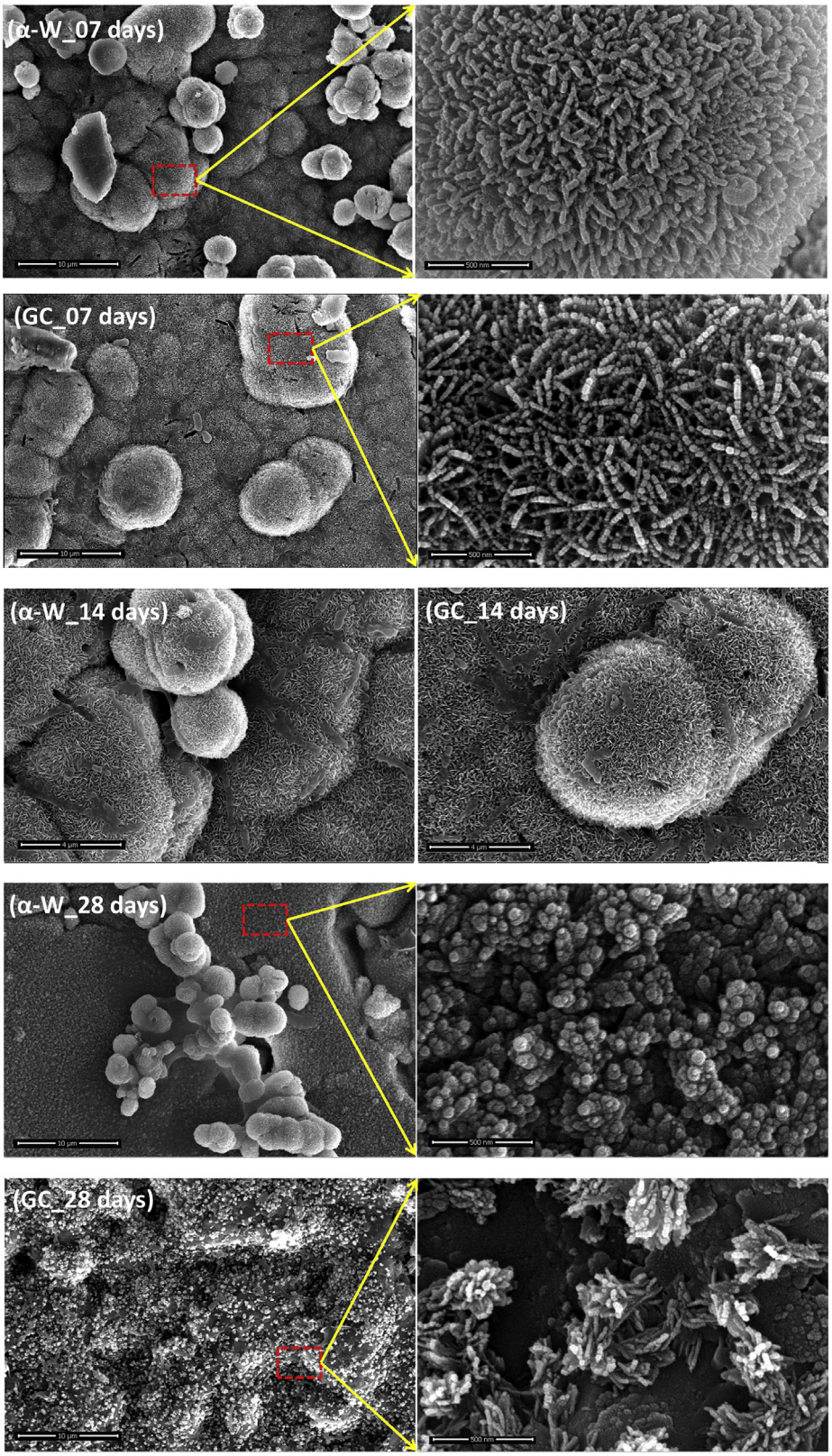

Fig. 10. SEM micrograph of wollastonite and glass-ceramic after soaking in SBF solution for 7days, 14 days and 28 days.

$$CaSiO_3(s) + OH^-(aq.\ ) \rightarrow SiO_3(OH)_3^-(aq.\ ) + Ca^{2+}(aq.\ ) \quad (6)$$

$$CaSiO_3(s) + H_2O(aq.\ ) \rightarrow HSiO_3^-(aq.\ ) + Ca^{2+}(aq.\ ) + OH^-(aq.\ ) \quad (7)$$

$$CaSiO_3(s) + H_2O(aq.\ ) \rightarrow SiO_4^{4-}(aq.\ ) + Ca^{2+}(aq.\ ) + 2H^+(aq.\ ) \quad (8)$$

Reaction (5) is faster than other reaction due to the lowest Gibbs free energy and higher equilibrium constant [49]. Therefore, H^+ ions

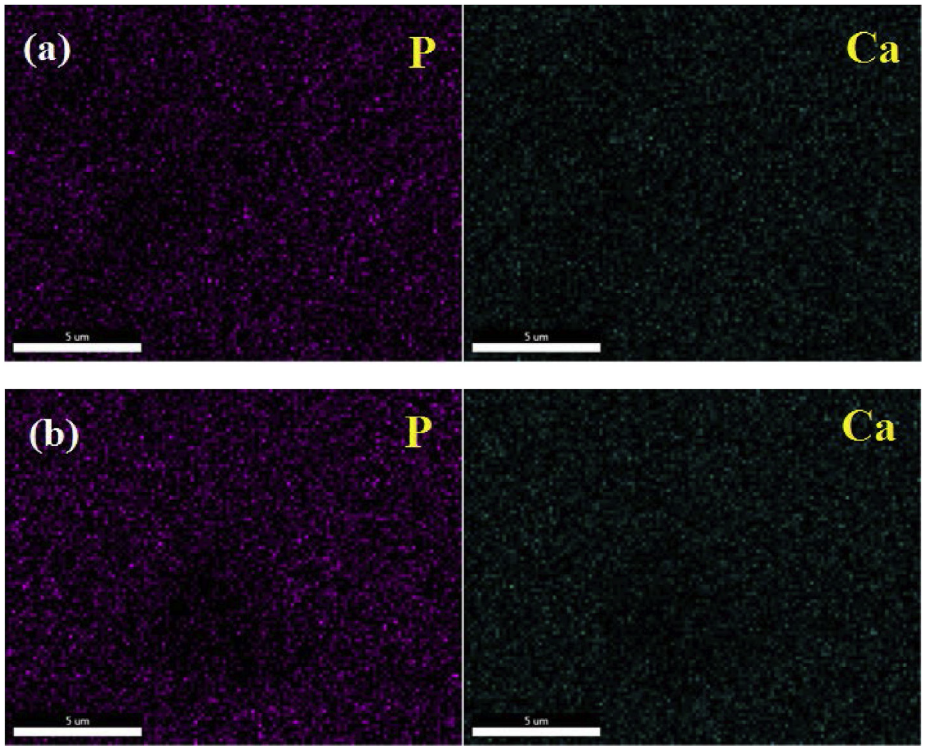

Fig. 11. Elemental mapping images for phosphorous (P) and calcium (Ca) of (a) wollastonite and (b) glass-ceramic after 28 days of soaking in SBF solution.

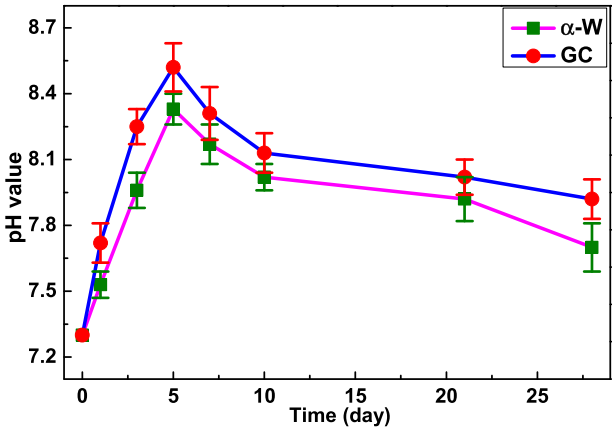

Fig. 12. Variation of pH value in SBF solution during soaking of wollastonite and glass-ceramic specimens.

deficiency may occur in the SBF solution, and it is enhancing the pH value. Subsequently, the pH value gradually decreases after 5 days of soaking for both the samples. It may be happened due to apatite layers, which are starting to deposit on the surface of the material through the absorption of phosphate (PO_4^{3-}) and carbonate (CO_3^{2-}) ions from the SBF solution. Therefore, phosphate (HPO_4^{2-}) and carbonate (HCO^{3-}) ions in the SBF may be decomposed as: $HPO_4^{2-} \rightarrow PO_4^{3-} + H^+$ and $HCO^{3-} \rightarrow CO_3^{2-} + H^+$ [14]. These reactions are increased the H^+ ion concentration in the system and decreased the pH value. Consequently, the pH value of the GC containing SBF is exhibited slightly higher than α-W containing the solution. The rate of Ca^{2+} ion exchange may be high in $CaSiO_3$ glass-ceramic than pure crystalline $CaSiO_3$. It results in more HA formation on the GC specimens, as shown in XRD (Figs. 5 and 6), FTIR (Figs. 7 and 8) and SEM (Fig. 10). Generally, glass-ceramic is retaining an asymmetrical structure, and the entropy is higher than crystalline materials. It is responsible for releasing the ions for decreasing the total energy of the system.

The apatite layer formation on the wollastonite is very much dependant on the releasing rate of Ca and Si ions from the material when it is immersed in SBF solution [49]. The mechanism of HA formation on the wollastonite surface is graphically illustrated in Fig. 13. First silica (≡Si–OH) reach surface is developed through the reaction of (5), and this is demonstrated a negative charge on the surface with (≡Si–O^-) functional groups. The (≡Si–O^-) groups can promote the formation of heterogeneous nucleation of HA through the absorbing of calcium and phosphate ions from the surrounding. The amount of HA deposition on the surface spontaneously increases with soaking time by consuming the requisite ions, which is verified through EDX analysis, as shown in Fig. 14. The amount of P is increased, and Si is gradually decreased with soaking time from 7 to 28 days. It is demonstrated the growth of the HA layer on the material surface. The Ca/P ratio of α-W and GC after 28 days of soaking is 1.52 and 1.65, respectively. This data indicates that the α-W surface is containing a calcium-deficient HA (CDHA) because the stoichiometry ratio of Ca/P in HA is around 1.67. However, the Ca/P ratio of the GC surface is nearly stoichiometry ratio apatite. It may be ascribed due to higher ion exchange capability of GC than α-W. Therefore, GC immersed SBF contains more Ca^{2+} ions, and it eliminates the deficiency of Ca ions for formation of HA.

3.4. Hemolysis assay analysis

Hemolysis of blood cells is a destructive event. It could be taken place when the blood cell comes in contact with certain foreign materials. Thus, it is essential to analyze the *in vitro* blood compatibility of biomaterials before clinical applications. Fig. 15 (a) displays the % of hemolysis occurred by α-W and GC for 5 mg/ml concentration. Both samples exhibit fewer hemolysis values than the threshold value (< 2%) [34]. The visual inspection of the micro-centrifuge tubes is also shown in Fig. 15(b). It shows that the color of α-W and GC containing tubes are similar to the negative control (-ve) tube. These results demonstrate that both specimens are non-hemolytic. However, GC (1.928 %) sample is exhibiting the slightly higher value of hemolysis than α-W (1.505%). It is ascribed due to GC sample, which is leaching more

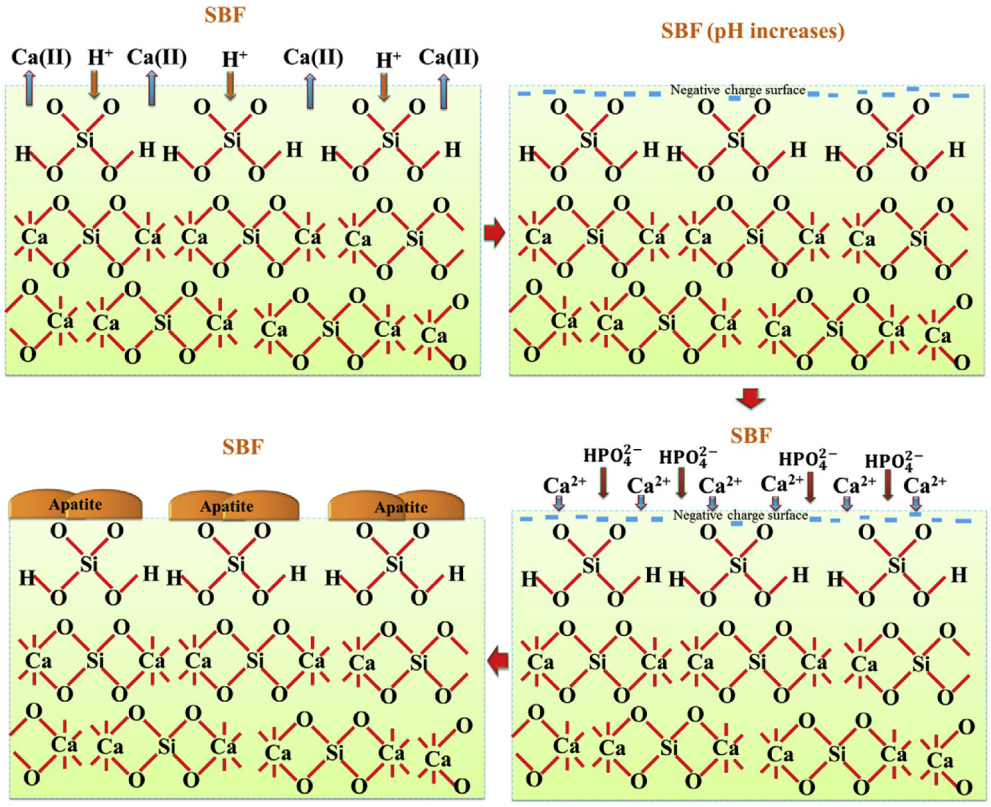

Fig. 13. Schematic representation of apatite formation mechanism for wollastonite in SBF solution [50].

cationic particles in the solution and helps to damage the cells [51]. Fig. 16 shows the microscopic observation of the red blood cells (RBC) aggregation after incubation. These pictures display that the α-W and GC samples perform similar to the negative control (-ve) and exhibit very less aggregation of the RBC cells with very little hemolysis in both the samples. Conversely, positive control (+ve) is completely

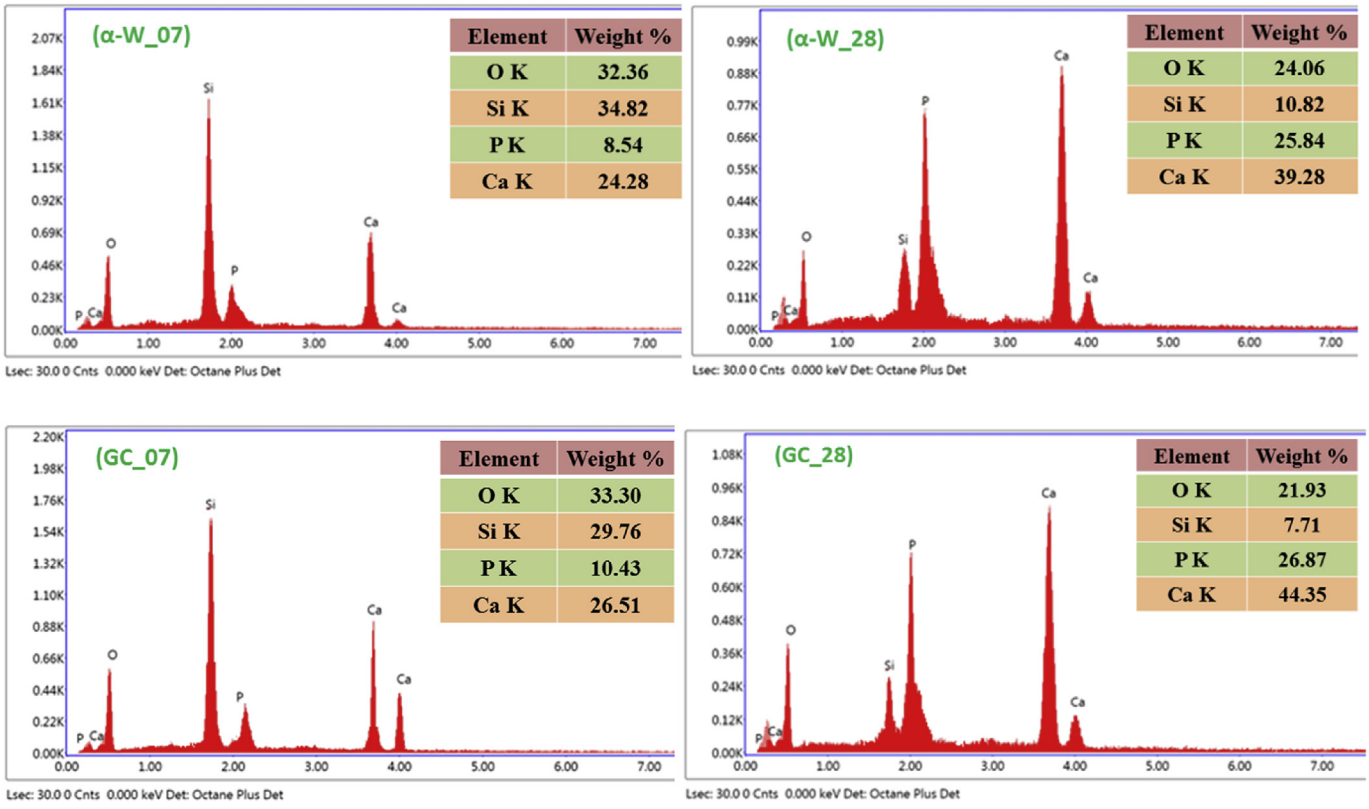

Fig. 14. EDX analysis of wollastonite and glass-ceramic after 7 days and 28 days.

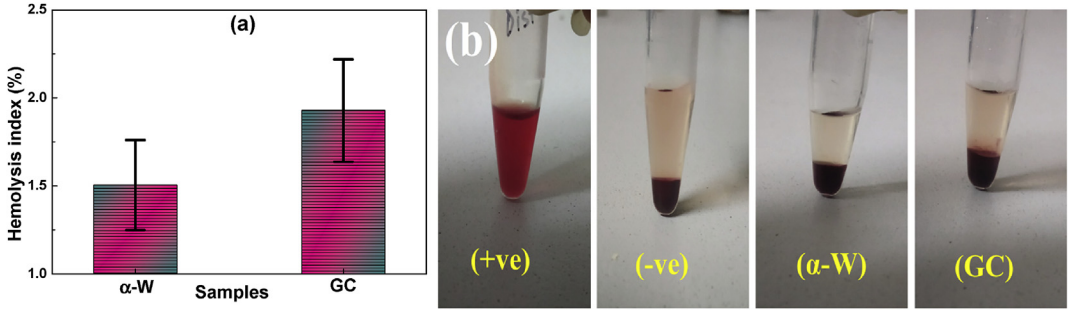

Fig. 15. (a) Hemolysis index of wollastonite and glass-ceramic specimens and (b)Visualinspection of the micro-centrifuge tubes after incubation.

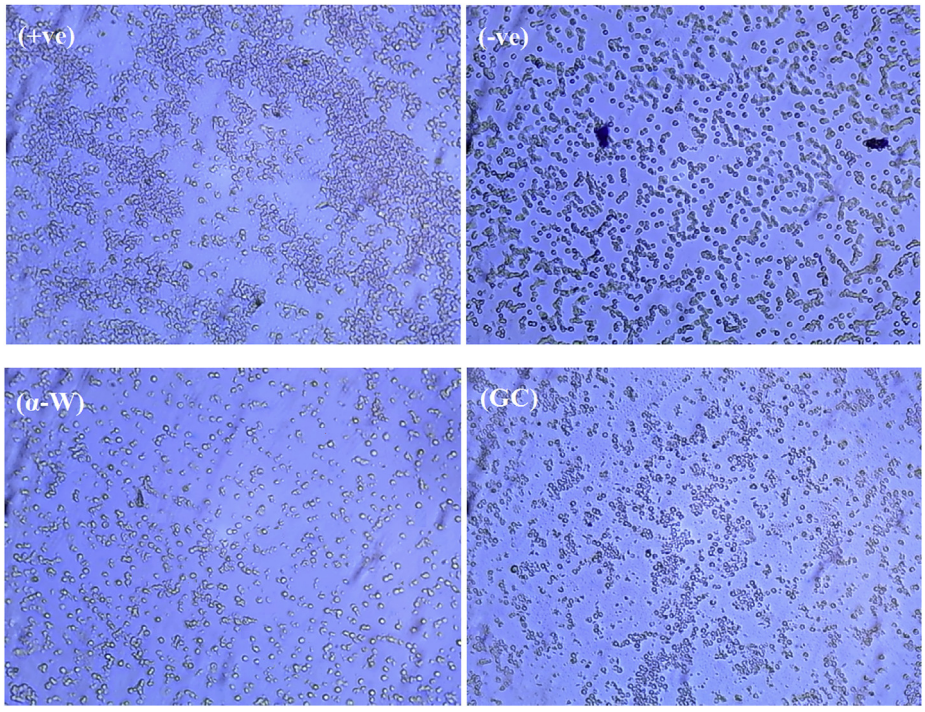

Fig. 16. Micrographs of RBC cells after incubation with +ve and -ve control, wollastonite and glass-ceramic.

aggregated. Hence, the waste-derived α-W, and GC is non-toxic, when these are contacted with blood.

4. Conclusions

Based on the results obtained in the present investigation, it is found that the waste RHA derived nano SiO_2 and chicken eggshells derived CaO can be used for preparing high purity wollastonite and glass-ceramic for biomedical applications. The physic-mechanical and bioactivity properties of α-W and GC have been comparatively investigated, and the following results are obtained:

- At 1200 °C sintered sample of chicken eggshells derived CaO (~99%), and rice husk ash (RHA) derived nano SiO_2 (~99%) mixture containsthe pseudo wollastonite, i.e., α-wollastonite (anorthic, C-1) as a major phase.
- At 1200 °C heat-treated wollastonite glass is composed of collaborative pseudo wollastonite (CI %~35) and amorphous phases.
- α-W and GC both have exhibited dense microstructure, but the density and bending strength of GC are slightly higher than α-W.
- The XRD, FTIR, and SEM analysis has suggested that the wastes derived α-W and GC both have excellent bioactivity.
- The surface of both the samples is fully covered by worm-like apatite particles (diameter < 30 nm) after 7 days of soaking in SBF solution. α-W shows a dense layer with nearly spherical in shape apatite particles and GC attributes a rough surface of amorphous layers and needle-like crystalline apatites after 28 days.
- The α-W surface contains a calcium-deficient HA (CDHA), and GC has maintained the stoichiometry ratio of Ca/P in HA.
- Both wastes derived specimens show good blood compatibility, i.e., hemolysis index is lower than 2% for 5 mg/mL concentration.

This study suggested that the GC shows more favorable physico-mechanical and bioactivity properties for biomedical applications than α-W.

Acknowledgments

The authors gratefully acknowledge all the faculty and staff of Department of Ceramic Engineering, Indian Institute of Technology (BHU), Varanasi, India and the Ministry of Human Resource Development (MHRD), Govt. of India for providing appreciable support.

Nomenclature

RH	Rice husk
RHA	Rice husk ash

α-W	Pseudo-wollastonite
GC	Glass-ceramic
XRD	X-ray diffraction
SEM	Scanning electron microscopy
HA	Hydroxyapatite
SBF	Simulated body fluid
AP	Apparent porosity
BD	Bulk density
FTIR	Fourier transform infrared spectrometer
CI	Crystallinity

References

[1] Deer, Howie, Zussman, second ed., Rock Forming Minerals; Single Chain Silicates 2A The Geological Society, London, 1997.

[2] P. Florian, F. Fayon, D. Massiot, 2J Si-O-Si Scalar Spin-Spin coupling in the solid state: crystalline and glassy wollastonite $CaSiO_3$, J. Phys. Chem. C 113 (2009) 2562–2572.

[3] S. Sen, first ed., Ceramic Whitewares: Their Technologies and Applications vol. 169, Oxford & IBH publishing co. pvt.Ltd, New Delhi, India, 1992.

[4] C. Wang, K. Lin, J. Chang, J. Sun, Osteogenesis and angiogenesis induced by porous β-$CaSiO_3$/PDLGA composite scaffold via activation of AMPK/ERK1/2 and PI3K/Akt pathways, Biomaterials 34 (2013) 64–77.

[5] S. Liu, F. Jin, K. Lin, J. Lu, J. Sun, J. Chang, K. Dai, C. Fan, The effect of calcium silicate on in vitro physiochemical properties and in vivo osteogenesis, degradability and bioactivity of porous β-tricalcium phosphate bioceramics, Biomed. Mater. 8 (2013) 025008.

[6] R. Sonntag, J. Reinders, J.P. Kretzer, What's next? Alternative materials for articulation in total joint replacement, Acta Biomater. 8 (2012) 2434–2441.

[7] C. Sarmento, Z.B. Luklinska, L. Brown, M. Anseau, P.N.D. Aza, S.D. Aza, In vitro behavior of osteoblastic cells cultured in the presence of pseudowollastonite ceramic, J. Biomed. Mater. Res. A 69 (2004) 351–358.

[8] K. Lin, M. Zhang, W. Zhai, H. Qu, J. Chang, Fabrication and characterization of hydroxyapatite/wollastonite composite bioceramics with controllable properties for hard tissue repair, J. Am. Ceram. Soc. 94 (2011) 206–212.

[9] S.F. Xu, K.L. Lin, Y.Y. Hu, Z. Wang, J. Chang, L. Wang, J.X. Lu, C.Q. Ning, Reconstruction of calvarial defect of rabbits using porous calcium silicate bioactive ceramics, Biomaterials 29 (2008) 2588–2596.

[10] I.H.M. Aly, L.A.A. Mohammed, S.A. Meer, K. Elsaid, N.A.M. Barakat, Preparation and characterization of wollastonite/titanium oxide nan fiber bioceramic composite as a future implant material, Ceram. Int. 42 (2016) 11525–11534.

[11] H. Li, D. Wang, C. Chen, F. Weng, H. Shi, Preparation and characterization of laser cladding wollastonite derived bioceramic coating on titanium alloy, Biointerphases 10 (2015) 031007 https://doi.org/10.1116/1.4929415.

[12] S. Saravanan, N. Selvamurugan, Bioactive mesoporous wollastonite particles for bone tissue engineering, J. Tissue Eng. 7 (2016) 1–6 https://doi.org/10.1177/2041731416680319.

[13] K. Lin, D. Zhai, N. Zhang, N. Kawazoe, G.G. Chen, J. Chang, Fabrication and characterization of bioactive calcium silicate microspheres for drug delivery, Ceram. Int. 40 (2014) 3287–3293.

[14] R. Shamsudin, F.A.A. Azam, M.A.A. Hamid, H. Ismail, Bioactivity and cell compatibility of β-wollastonite derived from rice husk ash and limestone, Materials 10 (2017) 1188.

[15] N. Zhang, J.A. Molenda, J.H. Fournelle, W.L. Murphy, N. Sahai, Effects of pseudowollastonite ($CaSiO_3$) bioceramic on in vitro activity of human mesenchymal stem cells, Biomaterials 31 (2010) 7653–7665.

[16] S.A. Saadaldin, S.J. Dixon, A.S. Rizkal, Bioactivity and biocompatibility of a novel wollastonite glass-ceramic biomaterial, J. Biomaterials Tissue Eng. 4 (2014) 1–8 https://doi.org/10.1166/jbt.2014.1261.

[17] L.A.N. Rodríguez, M.A.E. Romero, A.G. Álvarez, J.L.V. García, G.C.T. Munive, Evaluation of bioactive properties of α and β wollastonite bioceramics soaked in a simulated body fluid, J. Biomaterials Nanobiotechnol. 9 (2018) 263–276.

[18] R. Morsy, R. Abuelkhair, T. Elnimr, Synthesis and in vitro bioactivity mechanism of synthetic α-wollastonite and β-wollastonite, Bioceramics 7 (1) (2016) 65–70 https://doi.org/10.4416/JCST2015-00028.

[19] W. Höland, G.H. Beall, Handbook of Advanced Ceramics, Chapter 5.1 - Glass-Ceramics, Elsevie, 2013 371-38 https://doi.org/10.1016/B978-0-12-385469-8.00021-6.

[20] R.W. Andrews, Wollastonite, Natural Environment Research Council, Her Majesty's Stationery Office, London, 1970, p. 114.

[21] C.C. Chen, C.C. Ho, S.Y. Lin, S.J. Ding, Green synthesis of calcium silicate bioceramic powders, Ceram. Int. 41 (2015) 5445–5453.

[22] R. Puntharod, C. Sankram, N. Chantaramee, P. Pookmanee, K.J. Haller, Synthesis and characterization of wollastonite from egg shell and diatomite by the hydrothermal method, J. Ceram. Process. Res. 14 (2) (2013) 198–201.

[23] S. Vichaphund, M. Kitiwan, D. Atong, Microwave synthesis of wollastonite powder from eggshells, J. Eur. Ceram. Soc. 31 (2011) 2435–2440.

[24] F.A.A. Azam, R. Shamsudin, M.H. Ng, A. Ahmad, M.A.M. Akbar, Z. Rashidbenam, Silver-doped pseudowollastonite synthesized from rice husk ash: antimicrobial evaluation, bioactivity and cytotoxic effects on human mesenchymal stem cells, Ceram. Int. 44 (2018) 11381–11389.

[25] R.A. Rashid, R. Shamsudinn, M. Azmi, A. Hamid, A. Jalar, In-vitro bioactivity of wollastonite materials derived from limestone and silica sand, Ceram. Int. 40 (2014) 6847–6853.

[26] L. Fiocco, S. Li, E. Bernardo, M.M. Stevens, J.R. Jones, Highly porous polymer-derived wollastonite–hydroxycarbonate apatite ceramics for bone regeneration, Biomed. Mater. 11 (2016) 025016 https://doi.org/10.1088/1748-6041/11/2/025016.

[27] M. Sarangi, S. Bhattacharyya, R.C. Behera, Effect of temperature on morphology and phase transformations of Nano crystalline silica obtained from rice husk, Phase Transitions 82 (5) (2009) 377–386.

[28] S. Zafar, Rice straw as bionery Resource, Bio Energy Consult 26 (2015), http://www.bioenergyconsult.com/tag/rice-straw.

[29] S.S. Hossain, L. Mathur, P.K. Roy, Rice husk/rice husk ash as an alternative source of silica in ceramics: a review, J. Asian Ceram. Soc. 6 (4) (2018) 299–313 https://doi.org/10.1080/21870764.2018.1539210.

[30] S.M. Naga, H.H. El-Maghraby, M. Sabed, Highly porous scaffolds made of nanosized hydroxyapatite powder synthesized from eggshell, J. Ceram. Sci. Technol. 6 (2015) 237–244.

[31] S.S. Hossain, L. Mathur, A. Bhardwaj, P.K. Roy, A facile route for the preparation of silica foams using rice husk ash, Int. J. Appl. Ceram. Technol. (2019) 1–9 https://doi.org/10.1111/ijac.13164.

[32] S. Krimm, A.V. Tobolsky, Quantitative X-ray studies of order in amorphous and crystalline polymers. Quantitative X-ray determination of crystallinity in polyethylene, J. Polym. Sci. 7 (1951) 57–76.

[33] T. Kokubo, H. Takadama, How useful is SBF in predicting in vivo bone bioactivity? Biomaterials 27 (15) (2006) 2907–2915.

[34] ASTM F 756-00, American Society for Testing and Materials,Standard Practices for Assessment of Haemolytic Properties of Materials, Philadelphia, (2000).

[35] S.S. Hossain, P.K. Roy, Studies on physical and dielectric properties of bio-wastes derived synthetic wollastonite, J. Asian Ceram. Soc. 6 (3) (2018) 289–298.

[36] F.H.G. Leite, T.F. Almeida, R.T. Faria-Jr, Synthesis and characterization of calcium silicate insulating material using avian eggshell waste, Ceram. Int. 43 (2017) 4674–4679.

[37] S. Mor, C.K. Manchanda, S.K. Kansal, K. Ravindra, Nanosilica extraction from processed agricultural residue using green technology, J. Clean. Prod. 143 (2017) 1284–1290.

[38] S. Gu, J. Zhou, C. Yu, Z. Luo, Q. Wang, Z. Shi, A novel two-staged thermal synthesis method of generating nanosilica from rice husk via pre-pyrolysis combined with calcination, Ind. Crops Prod. 65 (2015) 1–6.

[39] W.M.N. Nour, A.A. Mostafa, D.M. Ibrahim, Recycled wastes as precursor for synthesizing wollastonite, Ceram. Int. 34 (2008) 101–105.

[40] J.R. Taylor, A.T.D. Insdale, Thermodynamic and phase diagram data for the CaO-SiO_2 system, Calphad 14 (1990) 71–88.

[41] 1 M. Singh, S. Lara, S. Tlali, Effects of size and shape on the specific heat, melting entropy and enthalpy of nanomaterials, J. Taibah Univ. Sci. 11 (2017) 922–929.

[42] S.R. Teixeira, A.E. Souza, C.L. Carvalho, V.C.S. Reynoso, M. Romero, J.M. Rincón, Characterization of a wollastonite glass-ceramic material prepared using sugar cane bagasse ash (SCBA) as one of the raw materials, Mater. Char. 98 (2014) 209–214.

[43] H.C. Li, D.G. Wang, C.Z. Chen, F. Weng, H. Shi, Influence of different amount of Na_2O additive on the structure, mechanical properties and degradability of bioactive wollastonite, Ceram. Int. 42 (2016) 1439–1445.

[44] Y. Pan, J. Yin, K. Zuo, D. Yao, Y. Xia, H. Liang, Y.P. Zeng, The sintering behavior and mechanical properties of $CaSiO_3$ bioceramics with B_2O_3 addition, Ceram. Int. 42 (2016) 9222–9226.

[45] C.J. Brinker, G.W. Scherer, Sol-Gel Science: the Physics and Chemistry of Sol-Gel Processing, Academic Press, 2013, p. 676.

[46] K. Rezwan, Q.Z. Chen, J.J. Blaker, A.R. Boccaccini, Biodegradable and bioactive porous polymer/inorganic composite scaffolds for bone tissue engineering, Biomaterials 27 (2006) 3413–3431.

[47] K. Lin, M. Zhang, W. Zhai, H. Qu, J. Chang, Fabrication and characterization of hydroxyapatite/wollastonite composite bioceramics with controllable properties for hard tissue repair, J. Am. Ceram. Soc. 94 (1) (2011) 99–105.

[48] K. Lin, C. Lin, Y. Zeng, High mechanical strength bioactive wollastonite bioceramics sintered from nano fibers, RSC Adv. 6 (2016) 13867–13872.

[49] M.M. Perdomo, Z.B. Luklinska, A.H.D. Aza, R.G. Carrodeguas, S.D. Aza, P. Pena, Bone-like forming ability of apatite–wollastonite glass ceramic, J. Eur. Ceram. Soc. 31 (2011) 1549–1561.

[50] X. Liu, C. Ding, P.K. Chu, Mechanism of apatite formation on wollastonite coatings in simulated body fluids, Biomaterials 25 (10) (2004) 1755–1761.

[51] M.A. Dobrovolskaia, J.D. Clogston, B.W. Neun, J.B. Hall, A.K. Patri, S.E. McNeil, Method for analysis of nanoparticle hemolytic properties in vitro, Nano Lett. 8 (8) (2008) 2180–2187.